

The effect of nonlinear quantum electrodynamics on relativistic transparency and laser absorption in ultra-relativistic plasmas

This content has been downloaded from IOPscience. Please scroll down to see the full text.

2015 New J. Phys. 17 043051

(<http://iopscience.iop.org/1367-2630/17/4/043051>)

View [the table of contents for this issue](#), or go to the [journal homepage](#) for more

Download details:

IP Address: 141.213.18.93

This content was downloaded on 18/06/2015 at 18:27

Please note that [terms and conditions apply](#).



PAPER

The effect of nonlinear quantum electrodynamics on relativistic transparency and laser absorption in ultra-relativistic plasmas

OPEN ACCESS

RECEIVED

13 December 2014

REVISED

6 March 2015

ACCEPTED FOR PUBLICATION

19 March 2015

PUBLISHED

24 April 2015

Content from this work
may be used under the
terms of the [Creative
Commons Attribution 3.0
licence](#).

Any further distribution of
this work must maintain
attribution to the
author(s) and the title of
the work, journal citation
and DOI.

Peng Zhang¹, C P Ridgers² and A G R Thomas³¹ Department of Nuclear Engineering and Radiological Sciences, University of Michigan, Ann Arbor, MI 48109-2104, USA² York Plasma Institute, Physics Department, University of York, UK³ Center for Ultrafast Optical Science and Department of Nuclear Engineering and Radiological Sciences, University of Michigan, Ann Arbor, MI 48109-2104, USAE-mail: agrt@umich.edu

Keywords: laser, plasma, strong field, radiation, pair production, QED, absorption

Abstract

With the aid of large-scale three-dimensional quantum electrodynamics (QED)-particle-in-cell simulations, we describe a potential experimental configuration to measure collective effects that couple strong field QED to plasma kinetics and develop a simple analytic model that describes the absorption due to radiation emission. For two counter propagating lasers interacting with a foil at intensities exceeding 10^{22} W cm⁻², a near-binary result occurs; when quantum effects are included, a foil that classically would effectively transmit the laser pulse becomes opaque. This is a dramatic change in plasma behavior, directly as a consequence of the coupling of radiation reaction and pair production to plasma dynamics.

1. Introduction

When the next generation of 10 PW lasers currently under construction are built [1–5], there are likely to be a few surprises in the way that they interact with matter. At the extreme intensities expected to be reached in the laser focus ($>10^{22}$ W cm⁻²) matter is rapidly ionised and the electrons in the resulting plasma are accelerated to such ultra-relativistic energies that the electric field they experience in their rest frame may reach the critical or Schwinger field of quantum electrodynamics (QED), $E_s = 1.3 \times 10^{18}$ V m⁻¹ [6]. This field is the threshold at which strong-field QED effects start to become important [7–10]. The new plasma state that is created is similar to that thought to exist in extreme astrophysical environments including the magnetospheres of pulsars and active black holes [11, 12]. Here, collective plasma processes are strongly affected by pair creation and radiation reaction [10, 13–17]. For brevity we will describe the resulting state as a ‘QED plasma’.

In non-relativistic plasma, electromagnetic waves with frequency ω_0 lower than the plasma frequency $\omega_{pe} = (n_e e^2 / m_e \epsilon_0)^{1/2}$, where n_e is the electron number density, cannot propagate through the plasma. The critical density n_c is the density at which the plasma frequency equals the wave frequency and above which the plasma is described as ‘overdense’. In the ultra-relativistic regime, electrons in the plasma are accelerated by the laser fields to such high energy that their effective mass is much greater than their rest mass. Consequently the plasma frequency is reduced by a factor $1/\sqrt{\langle\gamma\rangle}$, where $\langle\gamma\rangle$ is the average Lorentz factor of the electrons. An opaque (and nominally overdense) plasma may therefore be expected to become transmissive if the laser intensity, and therefore $\langle\gamma\rangle$, is sufficiently high. This ‘relativistically induced’ transparency [18, 19] optically switches the plasma from opaque to transparent and enables light propagation.

However, as the electromagnetic fields increase and we enter the QED-plasma regime, radiation reaction becomes significant, the electron motion is damped and hence $\langle\gamma\rangle$ may be expected to be reduced. Furthermore, radiation reaction leads to absorption of the electromagnetic wave [20] and as we will show, this is the more important effect. At even greater intensities, pair plasma may be produced by two step process [7] that is sufficiently dense to shield the laser fields. For greater intensities still, exceeding $I > 10^{25}$ W cm⁻² for 1 μ m lasers, higher order processes will start to become important [21]. As a result of these processes, a classical

prediction that a plasma is transmissive can be erroneous when QED effects are introduced. For 10 PW laser systems currently under development, understanding the interplay between QED effects and relativistic transparency will be important.

Consider a potential experiment with two counter propagating laser pulses of intensity in the range $10^{22} \text{ W cm}^{-2} < I < 10^{25} \text{ W cm}^{-2}$ with orthogonal linear polarizations impinging normally on both surfaces of a solid density foil, similar to the scenario of [22]. The radiation can be measured after the interaction with a calorimeter to determine the energy of the pulse after the interaction and because of the orthogonal polarizations, it can be determined what proportion of the radiation is reflected or transmitted. In this paper, we will show that, for an appropriate density/thickness foil, the laser radiation should be efficiently absorbed provided strong-field QED effects are considered in the plasma model, but if they are neglected the foil will be completely transmissive.

The structure of the paper is as follows. First we describe three-dimensional (3D) QED-particle-in-cell (QED-PIC) simulations of the interaction of two laser pulses with a thin foil target, demonstrating this dramatic effect. Then we use a series of 1D simulations to understand the scaling of the physics with laser/target parameters. Finally we develop a simple analytic model that captures accurately the overall trend with laser intensity of the absorption. Lastly we conclude and discuss the relevance to current and new future laser systems.

2. Numerical model

To model this experiment, we performed large-scale 3D numerical simulations using the QED-PIC code EPOCH [23–28], as shown in figure 1. EPOCH extends the Vlasov–Maxwell system to include the important QED processes in next generation laser-plasma interactions and is detailed in [24]. The electromagnetic field is split into high (i.e. gamma ray) and low (i.e. optical/plasma) frequency components. The low frequency components are coherent states that are unchanged in QED interactions [29]. The evolution of these macroscopic fields is determined by solving Maxwell’s equations. Electron and positron basis states are ‘dressed’ by these low-frequency fields, which are treated as a classical background that interacts with the charged particles and the high frequency component of the field, i.e. using the strong-field QED or ‘Furry’ representation [30]. We include the dominant first-order processes: gamma-ray photon emission by electrons and positrons and pair production by gamma-ray photons. Electron and positron motion is described by the ‘quasi-classical’ model of Baier and Katkov [31], i.e. the particles move subject to the Lorentz force on classical trajectories between point-like QED interaction events. Our model averages over photon polarization states, which has been shown to introduce a small error to the predicted pair-production rates [32].

3. Results

3.1. 3D QED-PIC simulation

Simulations were performed for two conditions: (1) ‘QED-off’, by which we mean no gamma-ray photons or pairs are generated and (2) ‘QED-on’, by which we mean that the QED-PIC code produces gamma-ray photons, tracks the photon’s dynamics and generates electron–positron pairs. The target is a $4 \mu\text{m}$ thick slab, with an initial density of $150 n_c$. The ion mass to charge ratio relative to the electron mass to charge ratio is taken as $(m_i/q_i)/(m_e/|q_e|) = 3674$. The lasers propagate in the $\pm x$ direction, as shown in figure 1(a). The left-hand side laser pulse is polarized in y direction and the right-hand side laser pulse is polarized in z direction. Both the laser pulses are of intensity $I = 4.5 \times 10^{23} \text{ W cm}^{-2}$, which is within the range expected to be reached by next-generation 10 PW lasers, with a gaussian profile of FWHM radius $4 \mu\text{m}$. Both laser pulses are 25 fs in duration (FWHM of temporal gaussian profile). The grid cell sizes (Δx , Δy , Δz) was $\lambda/25$, $\lambda/10$, $\lambda/10$, where λ is the laser wavelength. The time step was 0.99 of the Courant condition. 24 particles-per-cell were used. The boundaries were absorbing in the x direction and periodic in the y , z directions.

The radiation pressures of the laser pulses from opposite sides balance, such that the target is expected to be confined and centered around its initial position. However, it is compressed until the thermal pressure balances the ponderomotive pressure. After the laser pulses reached the surfaces of target foil, the foil was compressed inwards from both sides. For the QED-off simulation, when the peaks of the laser pulses arrived, both pulses started penetrating through the foil and eventually were transmitted. However, for the QED-on simulation, the laser pulses were blocked by the foil during the entire course of the simulation, indicating that relativistic transparency was suppressed by the QED effects. The magnitude of electric field E_y and the electron density profile are plotted at a time of 34τ , where τ is the laser period, in figures 1(b) and (c), for the QED-off and QED-on simulations, respectively.

Figure 2 displays the slice plots for the electron density in figures 1(b) and (c) through the center of the foil in both $x - z$ and $y - z$ planes. The electric field E_y along the x -axis ($y = 0$ and $z = 0$, i.e. the laser propagation

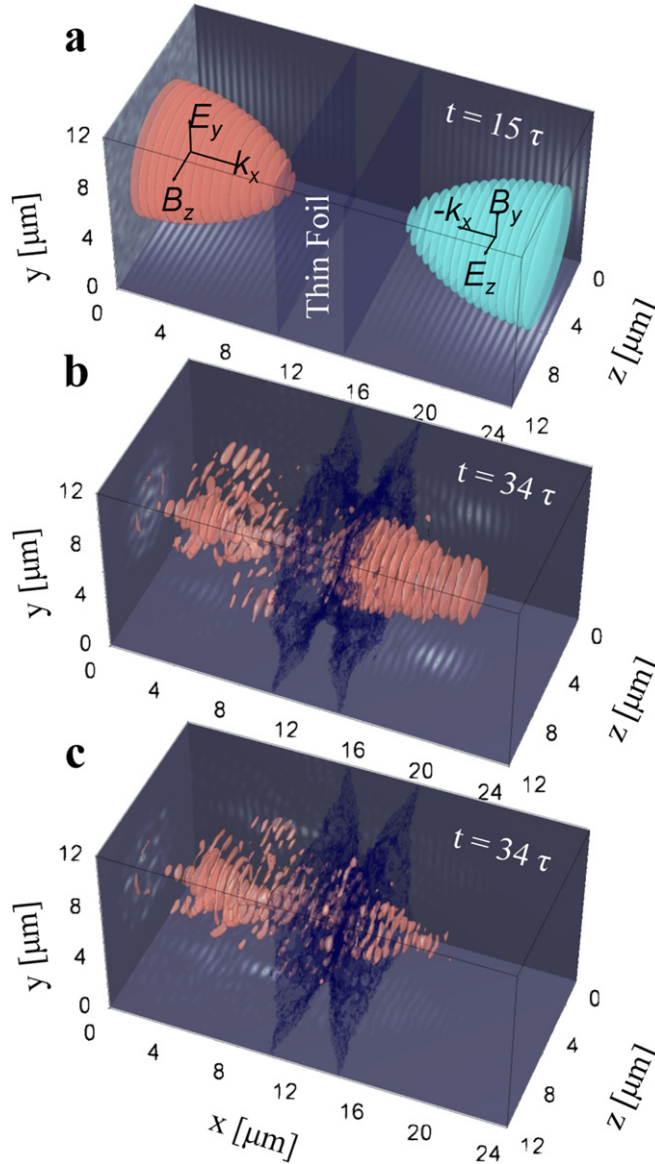
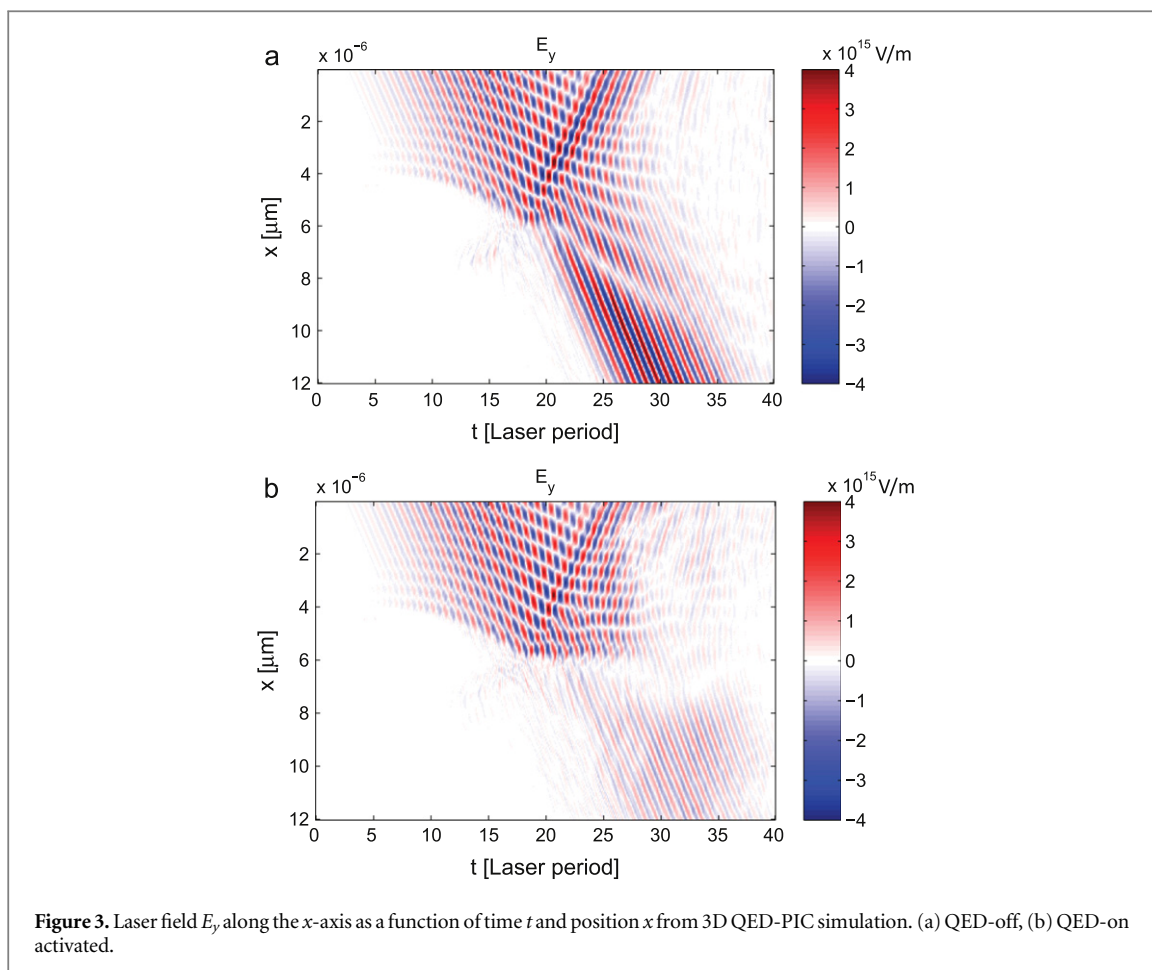
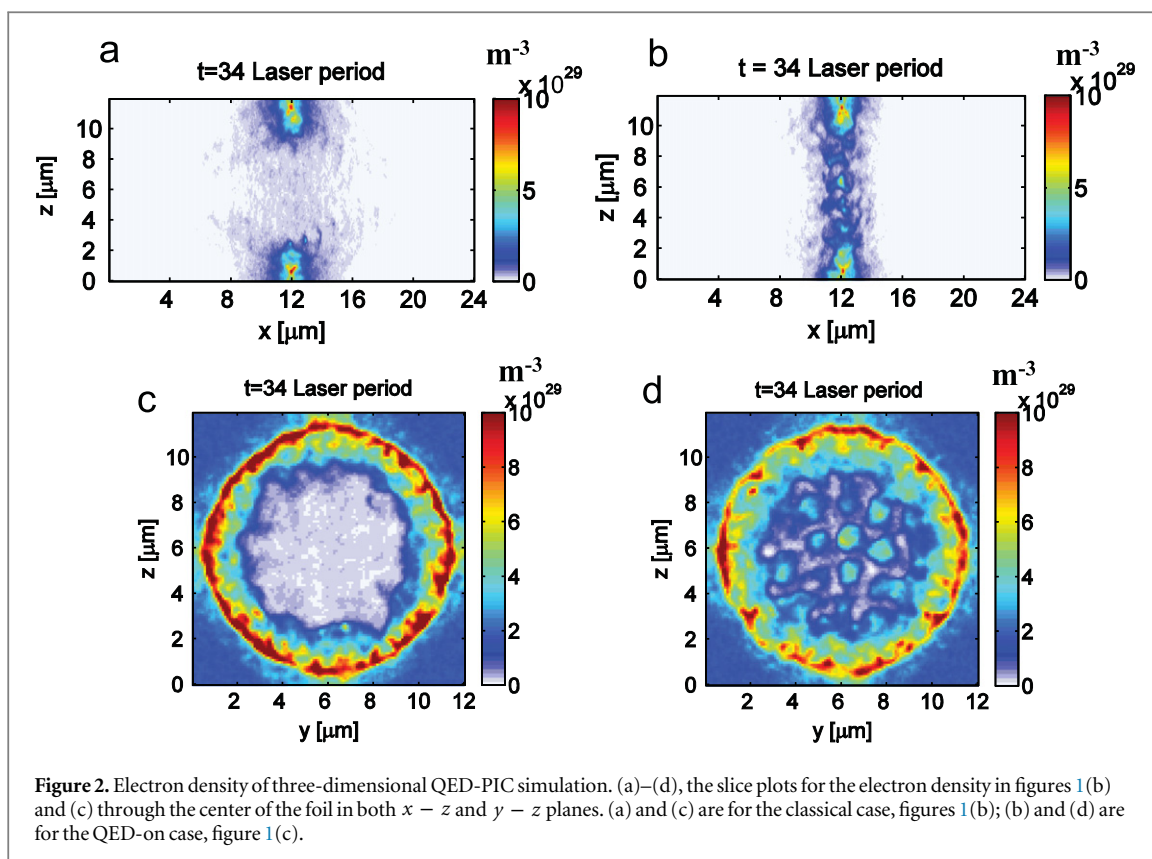


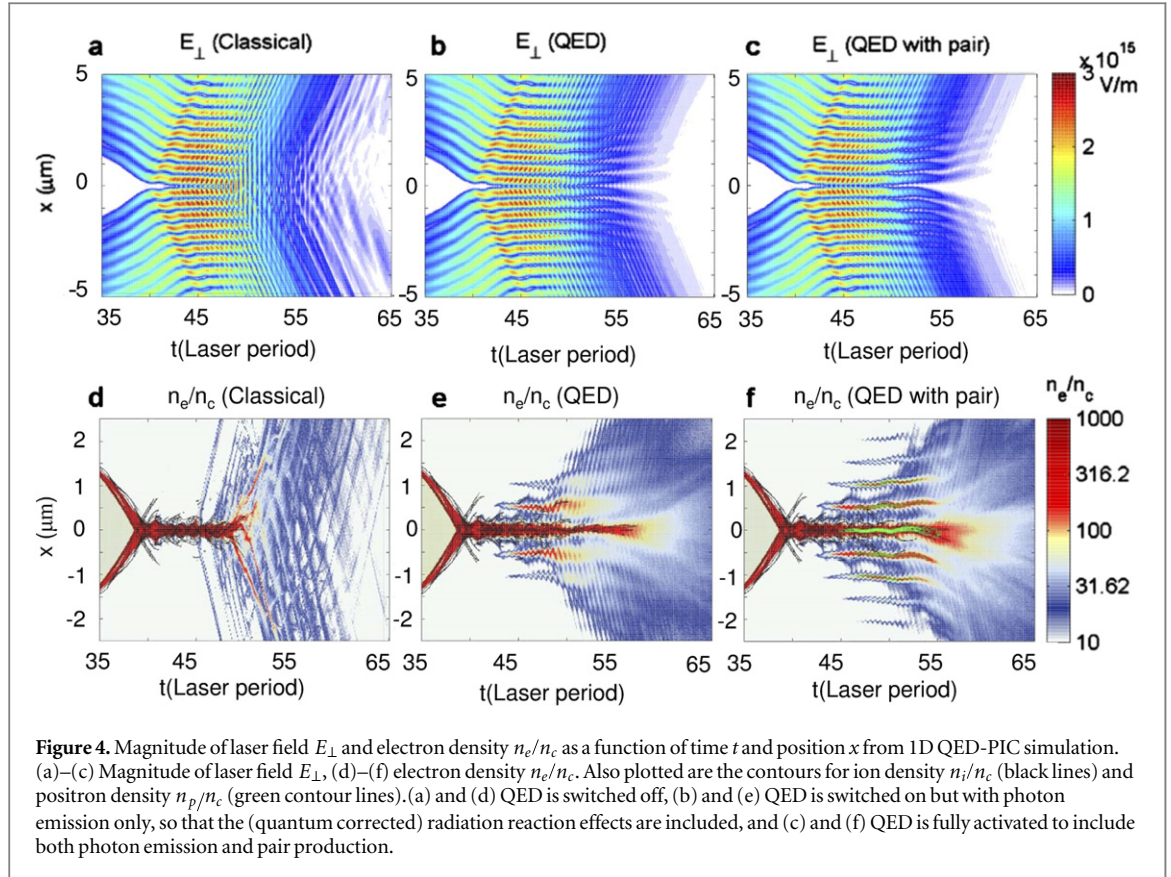
Figure 1. 3D QED-PIC simulation (a) two laser pulses illuminate a thin foil from both sides. The left pulse is linearly polarized in the y -direction, and the right pulse is linearly polarized in the z -direction. (b)–(c) The red isocontours show the magnitude of left pulse electric field, $|E_y|$ and the blue isocontours show the electron number density, all at $t = 34\tau$, for the QED-off and QED-on simulations, respectively. Side panels display slices of $E_{y(z)}$ through the planes that bisect the center of the box. The isocontours are taken at 33% of the maximum value.

direction) is plotted as a function of time t and position x , for both classical and QED-on simulations, as shown in figure 3. For both cases, the laser pulses initially pushed the target inwards. While the laser fronts moved inwards as a function of time, part of light was reflected. From $t = 18$ Laser period onwards, strong transmission occurred for the classical simulation. In contrast, the transmission is significantly suppressed for the QED-on simulation. It is interesting to note that though there are striking differences between the transmission of the pulse for the classical and QED simulations, the reflection of the pulses is quite similar, indicating that there is a *strong absorption of the laser power in the QED case*.

3.2. One-dimensional (1D) QED-PIC simulation

To facilitate comparison to the analytical scaling we develop later in this paper, we repeated the above simulation with circularly-polarized laser pulses, using 1D QED-PIC code calculations. For these, the grid cell size was $\Delta x = \lambda/100$ and the time step was 0.99 of the Courant condition. 960 particles-per-cell were used. The boundaries were absorbing. 3D and 1D behaviors are similar but not identical. In the 3D case, the tightly focused pulse slightly pushes the ions away from the axis, resulting in an effectively lower plasma density. Thus, to obtain equivalent results in the 1D simulation, the initial electron density is set to a lower value of $n_0 = 60n_c$, while all other parameters (except the polarization) are kept the same as the 3D case. The transmission behavior was





similar to the above 3D case. This is because the superposition of linear polarizations is similar to circular polarization in certain locations, in particular in the center of the domain where the plasma is located. The simulations were performed under three conditions: (1) QED-off; (2) QED-on with γ -ray photon generation only (the code is allowed to produce photons and calculates the recoil due to emitting photons, which gives the radiation reaction effect, but the photon is not tracked and thus no pair production occurs); and (3) QED-on with both gamma-ray photon and pair production.

The magnitude of the laser electric field and the plasma density are plotted as a function of time t and position x , as shown in figure 4, for all the three conditions. For all the three conditions, the laser plasma interaction process may be characterized by three distinct stages: an initial piston-like forward push of electrons by the laser illumination, followed by stagnation at the center between the two lasers and finally electron re-injection in the backward direction.

During the initial push, both electrons and ions are continuously compressed inwards until 40τ , as shown in figures 4(d)–(f). This compression process is almost identical under all the three conditions, implying that radiation reaction and QED effects are not important at this stage. This is because, in the case of a single laser beam hitting a charged particle at rest, the zero momentum frame of reference (ZMF), in which the charged particle has a periodic trajectory, does not coincide with the laboratory frame due to particle recoil. The ZMF moves in the direction of propagation of the laser beam with a velocity corresponding to a Lorentz factor equal to a [7, 33], where $a = eE/mc\omega_0$ is the normalized field strength. The laser frequency in the ZMF is thus redshifted compared to the laboratory frame. Because the strength parameter a is a Lorentz invariant, the reduced wave frequency in the ZMF implies a reduced amplitude of the wave field: $E_{RF} \approx E/a$ and hence the effects of radiation reaction and QED become reduced.

After the piston-like push of the electrons by laser, the bulk plasma stagnates when the ponderomotive pressure of the laser is balanced by the thermal pressure of the compressed plasma slab. We find that in this quasi-static phase of the two sided illumination only the electron motion needs to be considered since there is little bulk ion motion.

There was always a small portion of the electrons at the edge of the electron layer being accelerated back into the laser fields, regardless of whether QED effects are included or not. This is simply because hotter electrons can drift through the laser where the ponderomotive force and the force due to charge separation approximately balance. However, radiation reaction dramatically changes the dynamics of these back-injected electrons to radiatively cool them such that they get trapped in the nulls of the ponderomotive potential. These electrons

form equally spaced ultra-high-density thin electron and (for pair production switched on) positron layers, of approximately equal density, in the nodes of the standing wave formed by the incident and reflected wave, as shown in figures 4(e) and (f). These cause the plasma to become further optically opaque compared to the QED-off case, where the layers are not present and the plasma is transmissive. This is shown in figures 4(a)–(c).

4. Analytic model for absorption

The situation of electrons circulating in an electric field in the presence of a fixed ion background—which is similar to the stagnated layer discussed previously since bulk ion motion is prevented by the colliding geometry—readily lends itself to analytical solution. The force balance in the longitudinal direction (between the electrostatic force and ponderomotive force) means that to good approximation the bulk of the electrons circulate in the transverse direction under the influence of the transverse laser fields. Thus, the more straightforward, ‘zero-dimensional’, solution for a wave propagating in a homogeneous plasma is of relevance.

4.1. Dispersion relation in radiation damped, near critical density plasma

An equilibrium solution can be found for the wave equation for the laser

$$\frac{\partial^2 \mathbf{A}}{\partial t^2} - c^2 \nabla^2 \mathbf{A} = \frac{\rho_0}{\epsilon_0} (\mathbf{v}_i - \mathbf{v}_e),$$

with the electrons and ions co-rotating with constant γ transverse to the propagation.

Classically, the electron equation of motion in an electromagnetic field, including radiation reaction according to the Landau–Lifshitz prescription [34], is

$$m_e c \frac{d(\gamma \boldsymbol{\beta})}{dt} = \mathbf{F}_L - \tau_R \frac{\gamma^2 \boldsymbol{\beta}}{m_e c} \left| \mathbf{F}_L \right|_{\perp}^2, \quad (1)$$

where

$$\mathbf{F}_L = e \frac{d\mathbf{A}}{dt} - e (\nabla \mathbf{A}) \cdot \mathbf{v} + e \nabla \phi \quad (2)$$

is the force on a single electron expressed in terms of the vector and scalar potentials, $\tau_R = e^2 / (4\pi\epsilon_0 m_e c^3) = 6.245 \times 10^{-24}$ s and terms of order $1/\gamma^2$ and higher have been omitted [7]. In the radiation reaction expression, the second term on the right-hand side, only the force perpendicular to $\boldsymbol{\beta}$ contributes.

For a circularly polarized plane wave propagating in the $+\hat{z}$ direction with polarization direction unit vector given by $\hat{\mathbf{e}} = \mathcal{R} \left\{ e^{i(\omega_0 t - kz)} \right\} \hat{\mathbf{x}} + \mathcal{I} \left\{ e^{i(\omega_0 t - kz)} \right\} \hat{\mathbf{y}}$ such that $\mathbf{A} = (A_0/\omega_0) \partial \hat{\mathbf{e}}/\partial t$, for an appropriate choice of initial conditions, there are two components of the force on the electron. In the $\hat{\mathbf{e}}$ direction $F_{L,\hat{\mathbf{e}}} = e\omega A_0$, where $\omega = \omega_0 - kv_z$ and in the $\hat{\mathbf{z}}$ direction $F_{L,\hat{\mathbf{z}}} = e\mathbf{v} \cdot \partial \mathbf{A}/\partial z$. The small forward force is due to radiation reaction rotating the particle velocity away from parallel to the magnetic field.

We can therefore write the equation of motion for an electron in the circularly polarized plane wave as [7, 35]

$$\frac{d(\gamma \boldsymbol{\beta})}{dt} = \omega a \left\{ \hat{\mathbf{e}} - a\omega\tau_R\gamma^2\boldsymbol{\beta} \left[1 - (\boldsymbol{\beta} \cdot \hat{\mathbf{e}})^2 \right] \right\}. \quad (3)$$

In the more realistic situation of a plane wave incident on a foil, there will be a reflected component of the field also. For the superposition of 2 plane waves propagating in the $+\hat{z}$ and $-\hat{z}$ directions with polarization direction unit vector given by $\hat{\mathbf{e}} = \mathcal{R} \left\{ e^{i\omega t} \cos kz \right\} \hat{\mathbf{x}} + \mathcal{I} \left\{ e^{i\omega t} \cos kz \right\} \hat{\mathbf{y}}$ such that $\mathbf{A} = (A_0/\omega) \partial \hat{\mathbf{e}}/\partial t$, the situation is more complicated than before and there are three components of the force on the electron \mathbf{F}_L . In the $\hat{\mathbf{e}}$ direction $F_{L,\hat{\mathbf{e}}} = e\omega_0 A_0 \cos kz$, in the $\hat{\mathbf{z}} \times \hat{\mathbf{e}}$ direction $F_{L,\hat{\mathbf{z}} \times \hat{\mathbf{e}}} = ekv_z A_0 \sin kz$ and in the $\hat{\mathbf{z}}$ direction

$$F_{L\hat{\mathbf{z}}} = -e \frac{\partial \mathbf{A}}{\partial z} \cdot \mathbf{v} + e \frac{\partial \phi}{\partial z}. \quad (4)$$

It is a reasonable assumption that the longitudinal forces cancel at the point of reflection. That is to say the effective ponderomotive force and the force from charge separation between the electrons and ions cancel (we consider bulk ion motion effects in section 4.3). Otherwise, on the vacuum side of the interface electrons will be accelerated towards the bottom of the ‘ponderomotive potential wells’ in the standing wave pattern, i.e. nulls in the vector potential. For a particle traveling with velocity $v_z \simeq c$ in the wave in the vacuum region, such that $kv_z \simeq \omega_0$, the total transverse force on the particle is $F_{L,\perp} \simeq e\omega_0 A_0$. In this case, radiation emission will lead to energy loss that means the electron slows down and drops into the ponderomotive potential well to form the observed spikes.

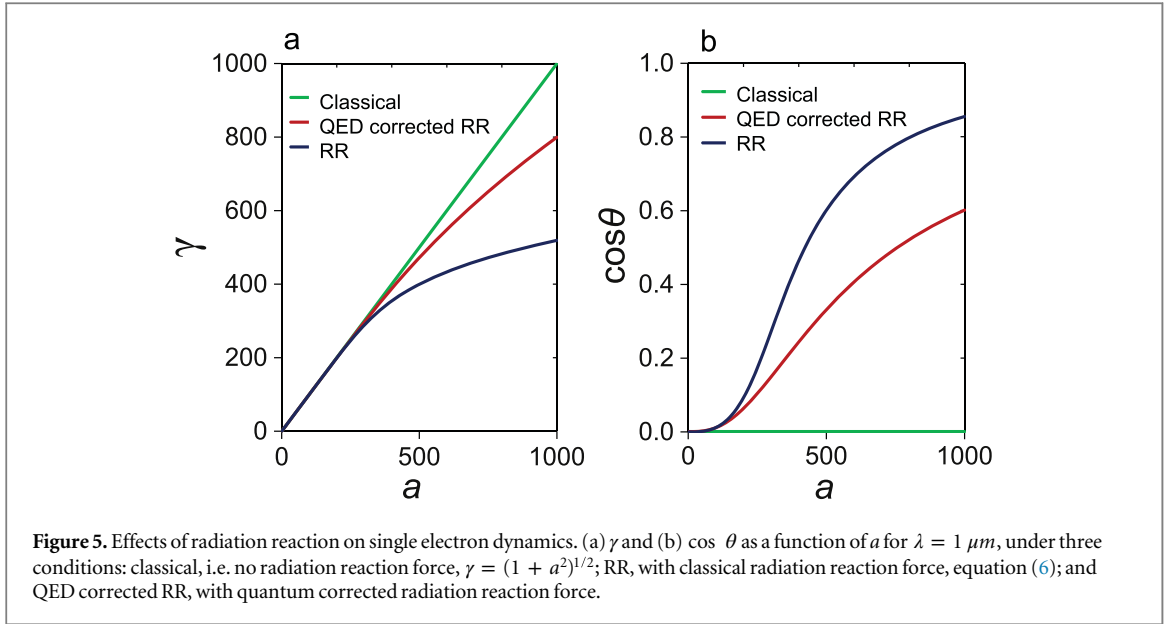


Figure 5. Effects of radiation reaction on single electron dynamics. (a) γ and (b) $\cos \theta$ as a function of a for $\lambda = 1 \mu\text{m}$, under three conditions: classical, i.e. no radiation reaction force, $\gamma = (1 + a^2)^{1/2}$; RR, with classical radiation reaction force, equation (6); and QED corrected RR, with quantum corrected radiation reaction force.

Finally, in plasma at close to critical density, the wavenumber is small $k \ll \omega$, and hence the only significant force is $F_{L,\hat{e}} = e\omega_0 A_0 \cos kz \approx e\omega_0 A_0$ whether there is a reflected wave present or not. These considerations are to show that for a circulating field, equation (3) is a reasonable approximation even in scenarios more complicated than the infinite plane wave in homogenous plasma.

An equilibrium solution to equation (3) exists where the component of the force parallel to $\boldsymbol{\beta}$ precisely compensates for the radiative momentum losses, while the perpendicular component provides the centripetal force for circular motion of the electrons. Setting the left-hand side of equation (3) to 0 [7], we find, by neglecting terms of order γ^{-2} or smaller

$$\gamma = a \sin \theta, \quad \Gamma \sin^2 \theta - \cos \theta = 0, \quad (5)$$

where $\Gamma = \tau_R \omega a \gamma^2$. Combining with equation (5) and eliminating θ , we obtain a relation between γ and a

$$\tau_R^2 \omega^2 \gamma^8 + \gamma^2 = a^2. \quad (6)$$

For ions, it is reasonable to assume no radiation reaction effects occur within the limits explored here and so $\mathbf{v}_i = q\mathbf{A}/\gamma_i m_i$, where $\gamma_i = \sqrt{1 + a^2 Z^2 m_e^2 / m_i^2}$.

It is well known [25, 36–38] that the classical description of an electron radiating in a strong electromagnetic field overestimates the total emitted power. This is connected to the fact that, in the quantum description, the emitted photon energy may not exceed the electron energy, whereas the classical approach does not have such a restriction. This effect may be approximately taken into account as follows. The total power of emitted radiation can be expressed as the power calculated from the classical description of radiation reaction, times a reducing factor $g(\eta)$ that accounts for truncation of the emitted spectrum [25, 37, 38], where $\eta = 1.286 \times 10^{-21} \omega a^2 \sin^2 \theta$ is the field strength relative to the critical field of QED in the particle rest frame. Equation (5) still holds, except that now $\Gamma = g(\eta) \omega \tau_R a \gamma^2$. Figure 5 shows the effect of this quantum-corrected radiation reaction force on both the electron Lorentz factor γ and the angle it makes with the laser polarization direction.

The significance of this expression can be seen by considering the resulting wave equation, which including the ion and electron current contributions yields a dispersion relation

$$\omega^2 = k^2 c^2 + \frac{\omega_{p0}^2}{\gamma} \left[\alpha + \frac{1}{1 - ig(\eta) \tau_R \omega \gamma^3} \right], \quad (7)$$

where $\alpha = Z\gamma m_e / \gamma_i m_i$ represents the ion contribution to the current. Without radiation reaction, as the vector potential is increased this ion contribution eventually equals the electron contribution (i.e. $\alpha \rightarrow 1$). However, the effect of radiation damping reduces the electron γ factor (and rotates the current vector) such that the ion contribution generally remains negligible compared with the electron contribution unless the laser wavelength is long ($\lambda \gg 1 \mu\text{m}$).

4.2. Asymptotic limits for $\sim 1 \mu\text{m}$ lasers

We can examine the behavior of dispersion relation equation (7) in two asymptotic limits for approximately $1 \mu\text{m}$ lasers, which is typical of current laser systems. Under these conditions, the ion contribution can be neglected

for the reasons given in section 4.1. For $\tau_R \omega \gamma^3 \ll 1$, i.e. weak (W) damping, the dispersion relation has a real component $\omega_R^{(W)} = \sqrt{k^2 c^2 + \omega_{p0}^2 / \gamma}$ and an imaginary component, i.e. representing *absorption* of the wave, of $\omega_I^{(W)} = \omega_{p0}^2 \tau_R \gamma^2 / 2$, with γ the Lorentz factor given by equation (6). Since in this limit the Lorentz factor is $\gamma \simeq a$, therefore the real part of the dispersion relation can be expressed as

$$\omega_R^{(W)} \simeq \sqrt{k^2 c^2 + \frac{\omega_{p0}^2}{a}} \quad (8)$$

and the imaginary part, representing wave absorption, is

$$\omega_I^{(W)} \simeq \frac{1}{2} \omega_{p0}^2 g(\eta) \tau_R a^2. \quad (9)$$

The real part yields a critical density for the threshold for wave propagation in the weak damping limit, i.e. where $k = 0$, of

$$n_c^{(W)} \simeq a n_{0c}, \quad (10)$$

where $n_{0c} = \omega_{p0}^2 m_e \epsilon_0 / e^2$ is the critical density of the plasma for very weak fields. This critical density is the same as that obtained in the absence of radiation reaction effects. In this limit the effect of radiation damping is only absorption of the electromagnetic wave.

In the strong (S) damping limit, $\tau_R \omega \gamma^3 \gg 1$, the dispersion relation yields an imaginary component

$$\omega_I^{(S)} \simeq \frac{\omega_{p0}^2}{2 \omega_0^2 g(\eta) \tau_R \gamma^4} \quad (11)$$

and since $\omega_{p0}^2 / (\gamma \omega_0^2) \gg 1$, the real part of the dispersion relation is

$$\omega_R^{(S)} \simeq \sqrt{k^2 c^2 + \frac{\omega_{p0}^4}{4 \omega_0^4 g^2(\eta) \tau_R^2 \gamma^8}}. \quad (12)$$

In this limit, equation (6) reduces to the Lorentz factor $\gamma \simeq [a / (\omega_0 g(\eta) \tau_R)]^{1/4}$ such that the absorption rate becomes

$$\omega_I^{(S)} \simeq \frac{\omega_{p0}^2}{2 \omega_0 a}. \quad (13)$$

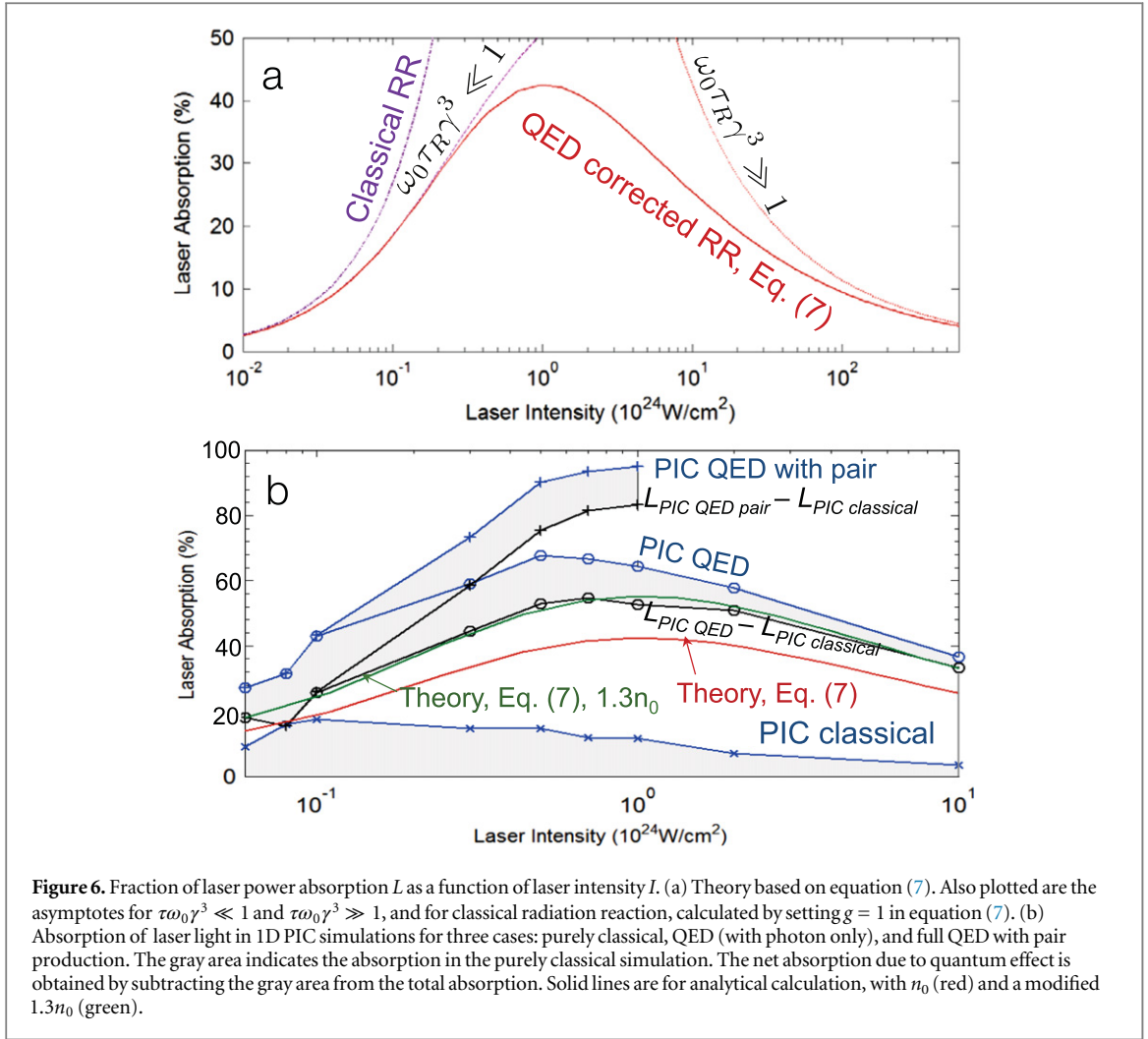
And from the expression for $\omega_R^{(S)}$, the critical density for wave propagation with frequency ω in the strong damping limit is

$$n_c^{(S)} \simeq 2 a n_{c0}, \quad (14)$$

which is a factor of 2 larger than that of weak damping limit, so it may be expected that radiation reaction *lowers* the threshold for relativistic transparency. However, for a laser at this critical frequency ($\omega_0 = \omega_c^{(S)}$) the wave is critically damped, i.e. $\omega_I^{(S)} = \omega_c^{(S)} = \omega_0$, and will therefore be attenuated in a single cycle. *Hence, effectively no relativistic transparency occurs as absorption dominates.*

In figure 6(a), we plot the fraction of laser energy absorption L as a function of the laser intensity I , calculated from $L = (\int \mathbf{j} \cdot \text{EdV}) / I \cong 4\pi \omega_I / \omega_0$, where \mathbf{j} is the current density, and ω_I is obtained from the full dispersion relation, equation (7). It is clear that when $I < 1 \times 10^{24} \text{ W cm}^{-2}$, L increases with intensity I . Around $1 \times 10^{24} \text{ W cm}^{-2}$, L reached its maximum. L subsequently decreases as I increases further. This is strikingly different from the classical radiation reaction calculation (i.e. no quantum correction), which predicts L increases continuously with I . The two asymptotic limits given above are also shown in the graph.

Figure 6(b) shows the absorption of the laser energy calculated directly from a series of 1D PIC simulations. In these simulations, the target density is $n_0 = 100 n_c$, and square shaped laser pulses with length of 30 laser cycles are used. When QED effects are included but pair production is not allowed, the scaling of L from simulation is very similar to that of theory, showing a maximum around $1 \times 10^{24} \text{ W cm}^{-2}$. The analytical curve fits the simulation the best when a density of $1.3 n_0$ is used, which may be partially explained by the fact that the plasma density is compressed during the laser plasma interaction. The functional shape of equation (7) is well reproduced. However, when pair production is activated, L increases continuously with I . For $I > 5 \times 10^{23} \text{ W cm}^{-2}$, L exceeded 90%. Note that L is calculated from the simulations relative to the total laser light, but the reflected fraction is not significantly changed by the addition of QED effects. Due to the extremely large absorption fraction, the effective laser field strength (therefore the Lorentz factor γ) is significantly reduced, resulting in the loss of relativistic transparency for the plasma. In addition, this absorption into electron–positron pairs may be of interest for the efficient production of dense laboratory pair-plasma [39, 40].



4.3. Absorption for one-sided illumination

Within the framework of our simple model for fixed target, equations (3)–(7), we may also evaluate the laser absorption properties for the case of single sided laser illumination of a dense plasma target. Under single sided illumination, the bulk target will be accelerated in the forward direction by light pressure. We can use our model for fixed ions in the instantaneous rest frame of the bulk plasma, assuming that the acceleration timescale is small compared with the laser period. The main effect will be that the laser frequency will be Doppler red-shifted in this frame. Since the laser strength parameter a is a Lorentz invariant, the reduced frequency implies a reduced amplitude of the wave electric field. Hence, QED effects are reduced such that the absorbed laser power fraction is also expected to decrease.

Consider the accelerating ion front to be moving in the \hat{z} direction with velocity $v_{iz} = \beta_{iz}c$, corresponding to a Lorentz factor γ_{iz} . In the instantaneous rest frame, the plasma frequency is $\omega'_{p0} = \omega_{p0}/\sqrt{\gamma_{iz}}$, the laser frequency is $\omega'_0 = \omega_0/[(1 + \beta_{iz})\gamma_{iz}]$, the QED strength parameter is $\eta' = \eta/\gamma_{iz}$ and a is a Lorentz invariant. The damping rates $\omega_I^{(W)}$, $\omega_I^{(S)}$ can be obtained from equations (9)–(13) in the instantaneous rest frame. Transforming these rates back to the laboratory frame, we obtain

$$\omega_I^{(W)} \simeq \frac{1}{2\gamma_{iz}^2} \omega_{p0}^2 g(\eta/\gamma_{iz}) \tau_R a^2, \quad (15)$$

$$\omega_I^{(S)} \simeq \frac{\omega_{p0}^2 (1 + \beta_{iz})}{2\omega_0 a \gamma_{iz}}. \quad (16)$$

These equations clearly show that the absorption will be greatly reduced by ion motion in the direction of the laser pulse propagation. The velocity of the ion front could be, for example, the hole boring velocity $v_{iz} = v_{HB}$ for a thick target (i.e., much larger than the skin layer in which ion acceleration by the space-charge field occurs) and is the light sail velocity $v_{iz} = v_{LS}$ for a thin target [41–43]. The significance for ion acceleration is that the

absorption will cause a reduction of the laser piston velocity, which will affect the maximum ion energies in radiation pressure acceleration [44, 45].

5. Conclusion

In summary, we have studied the interplay of QED effects and collective processes in plasmas generated by next-generation 10 PW lasers for critical density plasma. In particular we have derived a dispersion relation for electromagnetic wave propagation and shown that the damping of collective electron oscillations leads to strong absorption of the wave. This has dramatic consequences for relativistic transparency. QED-PIC simulations are performed to demonstrate that the relativistically transparent plasma may be converted to become optically opaque if QED effects become important in a colliding pulse geometry. Under experimental conditions, the two pulses may have intensity fluctuations that mean the center of momentum frame where the layer is stabilized is not the laboratory frame. However, reflected light will be Doppler shifted in this case. Measurements of the backscattered spectrum will enable diagnosis of intensity miss-match and allow correction of the resulting difference in transmission.

Our expressions should also apply to single sided illumination, provided the Doppler shift of the incident radiation due to plasma motion is taken into account. It should be noted that for very overdense targets the analysis in this paper is likely to greatly overestimate the absorption, since the field strength that interacts with the bulk of electrons at the target surface will be greatly lowered by the skin effect. We also note that 3D simulations were performed to provide experimental framework to test the relativistic transparency with strong radiation reaction and QED effects. These predictions may be tested using high-power lasers in the next few years.

Acknowledgments

This research was supported by the AFOSR Young Investigator Program through Grant No. FA9550-12-1-0310 and Grant No. FA9550-14-1-0309, and in part through computational resources and services provided by Advanced Research Computing at the University of Michigan, Ann Arbor. The EPOCH code was developed as part of the UK EPSRC funded projects EP/G054940/1.

References

- [1] Rus B *et al* 2013 *Proc. SPIE* **8780** 87801T
- [2] Mourou G A, Labaune C L, Dunne M, Naumova N and Tikhonchuk V T 2007 *Plasma Phys. Control. Fusion* **49** B667
- [3] Marklund M 2010 *Nat. Photonics* **4** 72–74
- [4] Gerstner E 2007 *Nature* **446** 16–18
- [5] Gerstner E 2010 *Nat. Phys.* **6** 638
- [6] Schwinger J 1951 *Phys. Rev.* **82** 664
- [7] Bell A R and Kirk J G 2008 *Phys. Rev. Lett.* **101** 200403
- [8] Fedotov A M, Narozhny N, Mourou G and Korn G 2010 *Phys. Rev. Lett.* **105** 080402
- [9] Bulanov S S, Esirkepov T Z, Thomas A G R, Koga J K and Bulanov S V 2010 *Phys. Rev. Lett.* **105** 220407
- [10] Nerush E, Kostyukov I Y, Fedotov A M, Narozhny N B, Elkina N V and Ruhl H 2011 *Phys. Rev. Lett.* **106** 035001
- [11] Goldreich P and Julian W 1969 *Astrophys. J.* **157** 869
- [12] Blandford R D and Znajek R 1977 *Mon. Not. R. Astron. Soc.* **179** 433
- [13] Timokhin A 2010 *Mon. Not. R. Astron. Soc.* **408** 2092
- [14] Ridgers C, Brady C S, Duclous R, Kirk J G, Bennett K, Arber T D, Robinson A P L and Bell A R 2012 *Phys. Rev. Lett.* **108** 165006
- [15] Ridgers C P, Brady C S, Duclous R, Kirk J G, Bennett K, Arber T D and Bell A R 2013 *Phys. Plasmas* **20** 056701
- [16] Kirk J, Bell A and Ridgers C 2013 *Plasma Phys. Control. Fusion* **55** 095016
- [17] Bulanov S V, Esirkepov T Z, Kando M, Bulanov S S, Rykovanov S G and Pegoraro F 2013 *Phys. Plasmas* **20** 123114
- [18] Kaw P and Dawson J 1970 *Phys. Fluids* **13** 472
- [19] Palaniyappan S *et al* 2012 *Nat. Phys.* **8** 763–9
- [20] Bashinov A and Kim A 2013 *Phys. Plasmas* **20** 113111
- [21] King B and Ruhl H 2013 *Phys. Rev. D* **88** 013005
- [22] Shen B and Meyer-ter Vehn J 2001 *Phys. Rev. E* **65** 016405
- [23] Brady C S and Arber T D 2011 *Plasma Phys. Control. Fusion* **53** 015001
- [24] Ridgers C P, Kirk J G, Duclous R, Blackburn T G, Brady C S, Bennett K, Arber T D and Bell A R 2014 *J. Comput. Phys.* **260** 273–85
- [25] Kirk J G, Bell A R and Arka I 2009 *Plasma Phys. Control. Fusion* **51** 085008
- [26] Sokolov I, Naumova N, Nees J, Mourou G and Yanovsky V 2009 *Phys. Plasmas* **16** 093115
- [27] Duclous R, Kirk J G and Bell A R 2011 *Plasma Phys. Control. Fusion* **53** 015009
- [28] Piazza A D, Hatsagortsyan K and Keitel C 2010 *Phys. Rev. Lett.* **105** 220403
- [29] Glauber R 1963 *Phys. Rev.* **131** 2766
- [30] Furry W 1951 *Phys. Rev.* **81** 115
- [31] Baier V and Katkov V M 1968 *Sov. Phys.—JETP* **26** 854
- [32] King B, Elkina N and Ruhl H 2013 *Phys. Rev. A* **87** 042117

- [33] Lau Y Y, He F, Umstadter D P and Kowalczyk R 2003 *Phys. Plasmas* **10** 2155
- [34] Landau L D and Lifshitz E M 1975 Course of theoretical physics-Pergamon international library of science, technology, engineering and social studies *The Classical Theory of Fields* 4th edn (Oxford: Pergamon)
- [35] Bulanov S V, Esirkepov T Z, Kando M, Koga J K and Bulanov S S 2011 *Phys. Rev. E* **84** 056605
- [36] Erber T 1966 *Rev. Mod. Phys.* **38** 626
- [37] Ritus V I 1979 *Tr. Fiz. Inst. Akad. Nauk SSSR* **111** 6
- [38] Thomas A G R, Ridgers C P, Bulanov S S, Griffin B J and Mangles S P D 2012 *Phys. Rev. X* **2** 041004
- [39] Chen H *et al* 2010 *Phys. Rev. Lett.* **105** 015003
- [40] Sarri G *et al* 2013 *Phys. Rev. Lett.* **110** 255002
- [41] Esirkepov T, Borghesi M, Bulanov S V, Mourou G and Tajima T 2004 *Phys. Rev. Lett.* **92** 175003
- [42] Robinson A P L, Gibbon P, Zepf M, Kar S, Evans R G and Bellei C 2009 *Plasma Phys. Control. Fusion* **51** 024004
- [43] Macchi A, Borghesi M and Passoni M 2013 *Rev. Mod. Phys.* **85** 751–93
- [44] Tamburini M, Pegoraro F, Piazza A D, Keitel C H and Macchi A 2010 *New J. Phys.* **12** 123005
- [45] Nerush E N and Kostyukov I Y 2015 *Plasma Phys. Control. Fusion* **57** 035007